Optimisation of star tracker orientation and attitude trajectories for space-to-ground optical communication on CubeSats

Joseph Thompson*, David McKeown
School of Mechanical and Materials Engineering
University College Dublin, Ireland
*Email: joseph.thompson@ucd.ie

***Abstract*—Optical communication systems promise a step-change in data return capability for CubeSats but introduce exceptionally demanding pointing requirements. In some cases, sub-milliradian level pointing of the satellite is required to successfully acquire a laser signal from the ground. This is further complicated by the relatively high angular velocities and angular accelerations of the satellite-to-ground target vector during a typical communication pass. Typically, star trackers are used to achieve the required attitude knowledge for initial acquisition of the laser signal from the ground, or for re-acquisition if the link is lost, due to cloud cover for instance. Therefore, availability of the star tracker throughout the full communication pass is desirable. For a given communication pass, star tracker availability can be maximised in two ways: first by minimising the angular velocity of the tracker, and second by minimising stray light from both the sun and the earth entering the tracker's field of view. During a communication pass, the requirement to point the laser boresight at the ground station constrains the attitude of the satellite in two out of three degrees of freedom. The unconstrained third degree of freedom is a rotation around the laser terminal boresight. The focus of the present work is on how this additional rotation may be used to optimise star tracker performance during a communication pass. A method is presented to minimise the angular velocity while avoiding sun and earth exclusion zones of the sensor, thereby maximising attitude estimation accuracy under dynamic conditions. Finally, from a mission design perspective the method above may be applied over the course of a full mission to all predicted communication passes to find the optimal orientation of the star tracker on the satellite. Developed strategies are tested via numerical simulations in MATLAB/Simulink.**

***Index Terms*—CubeSat, optical communications, star tracker, attitude guidance, exclusion zones, trajectory optimisation.**

I. Introduction

Optical communication is increasingly attractive for small satellites because it offers substantially higher data rates than conventional radio-frequency systems while reducing spectral congestion and improving link security. Recent demonstrations such as CLICK, TBIRD and QUBE show that compact optical terminals are now feasible on CubeSat-class platforms [1]–[3]. However, the narrow beam divergence associated with laser communication also makes the overall mission strongly dependent on spacecraft attitude control performance. Even when fine-pointing hardware is available inside the terminal, the body-pointing subsystem must typically place the terminal within a tight acquisition envelope and maintain sufficiently small attitude error throughout the pass [4], [5].

For a CubeSat with a body-fixed optical terminal, this leads to two coupled design problems. The first is an early-phase mission-analysis problem: how should the attitude sensors be configured so that optical communication passes are feasible and robust over the mission? The second is a trajectory-planning problem: during a particular pass, what body-pointing profile should the spacecraft follow in order to maximise estimation and control performance, and ultimately link availability? These two problems are usually treated separately. Mission-analysis studies often use simplified pointing assumptions and conservative sensor placement rules, while guidance studies typically assume a pre-decided fixed hardware configuration for which the commanded attitude trajectory must then be optimised. In practice, the two are strongly coupled because the chosen sensor geometry limits the feasible body orientations and trajectories, while the body motion determines the operating conditions and performance of the sensors.

A particularly important issue for optical communication CubeSats is star tracker placement. As one of the most accurate attitude sensors, a star tracker is typically required for the initial laser beam acquisition from an optical ground station. It may also be required at any subsequent time during a communication pass for recovery of the link after weather-related or other interruptions. Its performance is constrained by classical exclusion zones, defined by Sun and Earth keep-out angles, and also by image smear under angular motion. These effects depend not only on the tracker mounting location but also on the spacecraft attitude trajectory during a communication pass.

The space-to-ground tracking problem is also known as a staring attitude problem. Aligning the optical terminal boresight with the ground-station line of sight constrains two out of three rotational degrees of freedom, leaving a free rotation or roll about the laser boresight. Analytical staring attitude command generation has been studied for Earth-observation and ground-target tracking missions [6]–[8]. Constrained atti-

Research funded under the National Space Subsystems and Payloads Initiative (NSSPI), part of the Government of Ireland Disruptive Technologies Innovation Fund.

tude control and star tracker avoidance constraints have also been studied in related contexts [9]–[11]. However, in these studies full 3-DOF attitude trajectory commands are typically considered.

The present work focuses on how the free roll degree of freedom can be used to optimise attitude control performance during a communication pass. The contribution is not a full closed-loop ADCS design, but rather a framework to support sensor configuration and pointing-command generation. First, analytical expressions are used to describe the staring frame kinematics and the Sun/Earth exclusion geometry. These are combined with a simple but physically motivated model for star tracker performance (minimising angular velocity). The framework is then used to identify favourable body-roll angles for individual communication passes and to compare different star tracker mounting offsets over the course of a full mission.

The remainder of the paper is organised as follows. Section II defines the spacecraft attitude kinematics for space-to-ground target tracking. Section III derives the star tracker mounting and exclusion-zone geometry. Section IV describes a method for finding the fixed-roll angles over a single communication pass which maximise star tracker availability. Section V extends the analysis to optimal mounting angles for a star tracker over a full mission. Section VI presents sample numerical results that test the methods presented. Finally, section VII summarises the main conclusions and identifies future research directions.

II. Spacecraft attitude kinematics for space-to-ground tracking

A. Minimum angular velocity staring frame

First we derive analytical expressions for the kinematics of a staring attitude frame, which we will denote S. We follow the example in [8]. Let $\boldsymbol{\rho}$ denote the line-of-sight vector from the spacecraft to the ground station given by

$$\boldsymbol{\rho} = \mathbf{r}_{GS} - \mathbf{r}_{SC}, \tag{1}$$

where $\mathbf{r}_{GS}$ and $\mathbf{r}_{SC}$ are the positions of the ground station and satellite respectively in an Earth centred inertial frame. During a communication pass this is the desired direction of the optical terminal boresight, so we define the Z axis of the staring frame as

$$\hat{\mathbf{z}}_S = \frac{\boldsymbol{\rho}}{\|\boldsymbol{\rho}\|}. \tag{2}$$

This constrains the attitude in two degrees of freedom with the remaining degree of freedom being a rotation about $\hat{\mathbf{z}}_S$. This free rotation is resolved by introducing a reference vector $\mathbf{k}$ and defining

$$\hat{\mathbf{x}}_S = \frac{\hat{\mathbf{z}}_S \times \mathbf{k}}{\|\hat{\mathbf{z}}_S \times \mathbf{k}\|}, \tag{3}$$

$$\hat{\mathbf{y}}_S = \hat{\mathbf{z}}_S \times \hat{\mathbf{x}}_S \tag{4}$$

as the remaining X and Y axes of the staring frame. Note that this definition requires the vector $\mathbf{k}$ to have a non-zero component perpendicular to the boresight direction $\hat{\mathbf{z}}_S$ at all times. A direction cosine matrix representing the rotation from inertial frame to staring frame may then be written as

$$\mathbf{C}_{S/I} = \begin{bmatrix} \hat{\mathbf{x}}_S^T \\ \hat{\mathbf{y}}_S^T \\ \hat{\mathbf{z}}_S^T \end{bmatrix}. \tag{5}$$

Different choices of vector $\mathbf{k}$ will generate different staring commands as demonstrated in [8]. Here we will use a Minimum-Angular-Velocity (MAV) staring frame where the reference vector $\mathbf{k}$ can be written in integral form as

$$\mathbf{k}(t) = \mathbf{k}(t_0) + \int_{t_0}^{t} \boldsymbol{\omega}_S(\tau) \times \mathbf{k}(\tau)\, d\tau. \tag{6}$$

The vector $\mathbf{k}(t_0)$ defines the initial attitude a time $t = 0$. The resulting minimum angular velocity of the staring frame is

$$\boldsymbol{\omega}_{S/I} = \frac{\boldsymbol{\rho} \times \dot{\boldsymbol{\rho}}}{\|\boldsymbol{\rho}\|^2}. \tag{7}$$

This corresponds to zero angular velocity around the laser boresight at all times. In other words, from some initial staring attitude (defined by $\mathbf{k}(t_0)$) this staring frame tracks the LOS to the ground station while introducing no unnecessary spin about the boresight.

B. Body-fixed frame

We define the attitude of the spacecraft body frame B as the MAV staring frame S with an additional rotation ϕ_B about the boresight axis ($\hat{\mathbf{z}}_S$). This attitude can be represented by direction cosine matrix

$$\mathbf{C}_{B/I} = \mathbf{R}_z(\phi_B)\mathbf{C}_{S/I}, \tag{8}$$

$$\mathbf{R}_z(\phi_B) = \begin{bmatrix} \cos\phi_B & \sin\phi_B & 0 \\ -\sin\phi_B & \cos\phi_B & 0 \\ 0 & 0 & 1 \end{bmatrix}. \tag{9}$$

The angle ϕ_B will be referred to as the *body roll angle*. In this case the angular velocity of the body frame B about the boresight axis is simply $\dot{\phi}_B$. Fig. 1 shows the MAV staring frame (blue) and body-fixed frame (red).

III. Star tracker mounting and availability

We now consider a star tracker rigidly mounted in the spacecraft body frame with boresight represented by the unit vector $\hat{\mathbf{u}}_{ST}$. Without loss of generality, the star tracker boresight is assumed to be located in the body fixed XZ plane at a fixed offset angle δ_{ST} from the negative Z direction as shown in Fig. 1. Note that $\delta_{ST} = 0$ corresponds to the star tracker pointing directly opposite the laser boresight. For a given offset angle $0 \leq \delta_{ST} \leq 180^\circ$ the possible pointing directions of the boresight are parametrised by the body roll angle ϕ_B, creating a circle (shown in green). This will be referred to as the *star tracker pointing circle* or simply *pointing circle*.

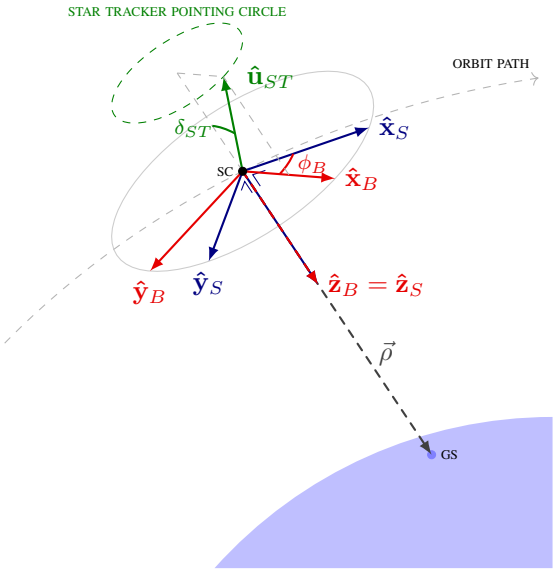

Fig. 1: The staring attitude frame and body-fixed frame showing star tracker mounting offset and star tracker pointing circle.

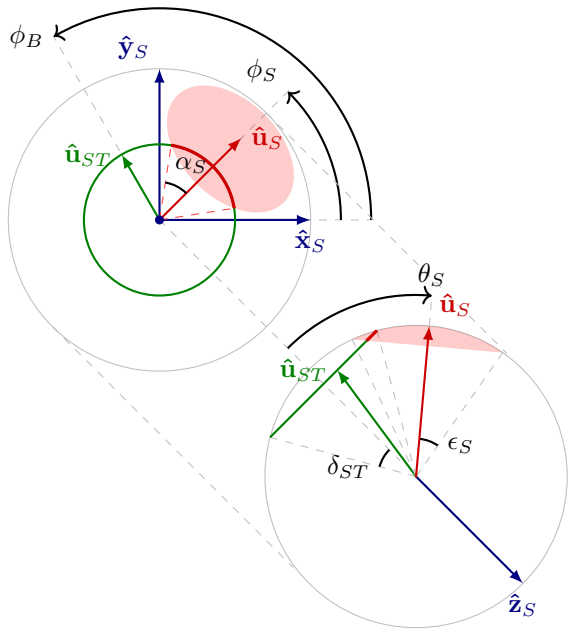

Fig. 2: The star tracking pointing circle and Sun and Earth exclusion zones in the minimum-angular-velocity staring frame.

A. Sun and Earth exclusion arcs

Let the unit vector $\hat{\mathbf{u}}_S$ denote sun direction in the staring frame. Figure 2 shows two projections of the unit sphere fixed in the staring frame, one of the XY plane and the second an orthogonal plane (lower right) that contains the staring frame Z axis and the sun vector $\hat{\mathbf{u}}_S$. The sun direction vector in the staring frame may be described in spherical coordinates by azimuth $0 \geq \phi_S < 2\pi$ and polar angle $0 \geq \theta_S < \pi$ as shown (Note that the polar angle θ_S is measured from the $-$Z direction). In addition, the star tracker boresight vector $\hat{\mathbf{u}}_{ST}$ is shown for some azimuth ϕ_B. Again the star tracker pointing circle is shown, which sits on the unit sphere, showing the possible pointing directions of $\hat{\mathbf{u}}_{ST}$.

For the star tracker we define κ_S as the Sun *keep-out angle*, which is considered a fixed instrument parameter obtained from manufacturer specifications. To ensure an attitude solution will be available from the star tracker, an angle of at least κ_S must be maintained between the star tracker boresight and the sun. The *sun exclusion half angle* for the star tracker may then be calculated as

$$\epsilon_S = \kappa_S + 0.27^\circ, \tag{10}$$

where 0.27° is the apparent angular radius of the sun from the satellite's point of view. Note the distinction between the keep-out angle which defines a minimum angle between the edge of the sun and the star tracker boresight, and the exclusion zone half angle which takes into account the angular size of the sun and defines a minimum angle between the centre of the sun and the star tracker boresight. Together the sun angle θ_S and the exclusion half angle ϵ_S define a spherical circular exclusion zone on the surface of the unit sphere. This is shown as the red shaded area in Fig. 2.

Under certain conditions, the sun exclusion zone and star tracker pointing circle intersect. We will call this intersection the *sun exclusion arc*, centred at an azimuth angle ϕ_S and with half angle α_S as shown. In general the exclusion arc half-width is given by

$$\alpha_S = \begin{cases} 0 & \epsilon_S \leq |\theta_S - \delta_{ST}| \\ \pi & \epsilon_S \geq \pi - |\pi - \theta_S - \delta_{ST}| \\ (\alpha_S)_\cap & \text{otherwise,} \end{cases} \tag{11}$$

where

$$(\alpha_S)_\cap = \cos^{-1}\left[\frac{\cos\epsilon_S - \cos\delta_{ST}\cos\theta_S}{\sin\delta_{ST}\sin\theta_S}\right]. \tag{12}$$

The first case corresponds to no intersection existing between the exclusion zone and pointing circle. Note that this includes the case where the exclusion zone half angle ϵ_S is smaller than the star tracker mounting offset angle δ_{ST} and $theta_S$ is such that the sun exclusion zone sits completely inside the star tracker pointing circle. The second case corresponds to the pointing circle lying completely inside the exclusion zone, so that the exclusion arc becomes a full circle. The third case is that shown in Fig. 2, where the sun exclusion zone partially intersects the star tracker pointing circle.

An exclusion half angle for the Earth may be calculated in a similar manner to that for the Sun giving

$$\epsilon_E = \kappa_E + \sin^{-1}\left(\frac{R_E}{\|\mathbf{r}_{SC}\|}\right), \tag{13}$$

where κ_E represents the Earth keep-out angle, which again is a specification of the star tracker. In this case the second term represents the apparent angular radius of the Earth (angle between the Earth horizon and nadir direction) assuming a spherical Earth with radius R_E. This value may be either

calculated at each instant in time from the actual spacecraft position or a conservative constant value may be used by substituting the perigee distance for $\|\mathbf{r}_{SC}\|$. An expression for the Earth exclusion arc half angle may be obtained by simply changing the subscripts in Eq. 12 from S to E.

B. Star tracker availability

The overall availability of the star tracker can be calculated by combining the Sun and Earth exclusion conditions. However, it should also be noted that whenever the sun is eclipsed by the Earth, sun avoidance is no longer necessary (a night-time pass). For this reason we introduce a modified version of the sun exclusion arc half angle which takes eclipses into account:

$$\alpha_S^* = \begin{cases} \alpha_S & f_e < 1 \\ 0 & f_e = 1, \end{cases} \tag{14}$$

where $0 \leq f_e \leq 1$ is the *eclipse fraction* which measures the extent to which the Earth is eclipsing the disc of the Sun from the satellite's point of view. In other words, the half angle of the sun exclusion arc α_S shrinks to zero whenever the sun is fully eclipsed by the Earth.

At any time t, the Sun and Earth exclusion arcs define forbidden intervals in roll angle, denoted $\mathcal{E}_S(t)$ and $\mathcal{E}_E(t)$, parametrised by their respective centres and half-widths $(\phi_S, \alpha_S^\star)$ and (ϕ_E, α_E). Therefore, when expressed in terms of these quantities, defined in the staring frame, the star tracker availability problem reduces naturally to a one-dimensional roll-feasibility problem over the angle ϕ_B. The allowable set of roll angles which guarantee tracker availability at time t is

$$\Phi(t) = [-\pi, \pi] \setminus (\mathcal{E}_S(t) \cup \mathcal{E}_E(t)), \tag{15}$$

where this allowable set may correspond to zero, one or two allowable arcs on the star tracker pointing circle.

IV. Feasible Roll Trajectory over a Single Communication Pass

The exclusion arc formulation introduced in the previous section enables the roll degree of freedom to be analysed independently of the cross-boresight motion. In this section, the problem of determining feasible roll trajectories over a single communication pass is considered, with particular focus on constant roll solutions. A fixed roll angle ϕ_B corresponds to zero roll rate and therefore minimises the additional angular velocity introduced by motion about the boresight. This may be beneficial for star tracker performance which is degraded at increased angular rates or, in the case of a spacecraft which is axisymmetric about the laser boresight axis, will result in zero control torque about that axis. Fixed-roll solutions may therefore be attractive from both a sensor performance and attitude control perspective.

A fixed roll angle ϕ_B is feasible at time t if $\phi_B \in \Phi(t)$. Over the duration of a communication pass, $t \in [t_0, t_f]$, the total availability associated with a given roll angle is defined as

$$J(\phi_B) = \int_{t_0}^{t_f} \chi(\phi_B, t)\, dt, \tag{16}$$

where

$$\chi(\phi_B, t) = \begin{cases} 1, & \phi_B \in \Phi(t), \\ 0, & \text{otherwise.} \end{cases} \tag{17}$$

The objective is to determine the set of roll angles that maximise $J(\phi_B)$. Depending on the relative motion of the exclusion arcs, several outcomes are possible. In some cases, there exists a continuous interval of roll angles that remains feasible for the entire pass. In other cases, no such interval exists, and the problem reduces to identifying roll angles that maximise partial visibility.

For numerical implementation, the problem above is evaluated over a discrete set of time samples. In this case, the availability function $J(\phi_B)$ becomes piecewise constant in ϕ_B, since its value can only change when ϕ_B coincides with a boundary of the allowable set $\Phi(t_k)$ at some time sample t_k. Between any two neighbouring boundary values, the feasibility of ϕ_B over the entire pass remains unchanged. This property allows the continuous optimisation problem to be reduced to the evaluation of a finite set of candidate roll angles. For each time t_k, the allowable set $\Phi(t_k)$ consists of one or more intervals within $[-\pi, \pi]$. The endpoints $\{b_i\}$ of these intervals are collected over the full duration of the pass and then sorted. Each consecutive pair of boundary values defines an interval $[b_i, b_{i+1}]$ within which $J(\phi_B)$ is constant. A single roll angle is selected from each interval as

$$\phi_{B,i} = \frac{b_i + b_{i+1}}{2}, \tag{18}$$

and the corresponding availability $J(\phi_{B,i})$ is evaluated. The optimal solution is then obtained by selecting the interval or intervals that maximise $J(\phi_B)$.

V. Optimising star tracker mounting angle

The fixed-roll analysis can be extended to determine an optimal mounting angle for a candidate star tracker. For a set of candidate mounting angles δ_{ST}, the procedure described in Sec. IV may be applied over all communication passes within a mission. The total availability for a full mission is then defined as

$$J_m(\delta_{\mathrm{ST}}) = \frac{\sum_{\text{passes}} J(\phi_B)_{\max}}{\sum_{\text{passes}} (t_f - t_0)}, \tag{19}$$

where $J(\phi_B)_{\max}$ is the maximum achievable availability for each pass. The optimal mounting angle is then obtained as

$$\delta_{\mathrm{ST}}^\star = \arg\max_{\delta_{\mathrm{ST}}} J_m(\delta_{\mathrm{ST}}). \tag{20}$$

From geometric considerations, the optimal mounting angle is expected to lie within the range

$$\epsilon_S \lesssim \delta_{\mathrm{ST}}^\star \lesssim \pi - \epsilon_E, \tag{21}$$

since for smaller angles Sun avoidance cannot always be achieved, while for larger angles Earth avoidance becomes infeasible.

VI. Numerical results

The proposed methods were evaluated numerically using MATLAB/Simulink. A satellite mission for a CubeSat in a 500km SSO over one year was simulated with the parameters shown in Tab. I. This was carried out in two stages. First, a simulation over the full mission duration was carried out using a coarse time step of 30 seconds to find all communication passes where the satellite reaches the minimum elevation for a duration of at least 30 seconds. Second, shorter simulations with a finer time step of 1 second were carried out for each individual communication pass. These simulations used simple models for 2-body orbit propagation (including J2 perturbations), Earth rotation, Sun position and eclipse. The simulation also calculated the direction cosine matrix representing the attitude of the zero velocity staring frame according to Eqs. 1-6. The initial value of reference vector $\mathbf{k}(t_0)$ was set to the position vector of the ground station relative to the centre of the Earth at the start of each communication pass so that the X axis of the staring frame lies roughly in the local horizontal plane at the ground station and the Y axis points roughly towards the Earth. For each communication pass, spacecraft position, ground station position, Sun direction, nadir direction, eclipse fraction and the staring frame DCM were computed and saved as time-series. The positions of both the Sun and Earth (nadir direction) were then converted to spherical coordinates $(\theta_S, \phi_S, \theta_E, \phi_E)$. A candidate star tracker with keep-out angles $\kappa_S = \kappa_E = 40°$ was considered with a mounting angle $\delta_{ST} = 45°$. Sun and Earth exclusion arcs for each communication pass were then calculated for this star tracker according to Eqs. 10-13. The intervals of body roll angle ϕ_B that achieve the greatest availability over each pass were then calculated using the procedure described in Sec. IV.

Plots that show the evolution of the exclusion arcs for the Earth and Sun over time were generated for each communication pass in the mission. As a sample, Figs. 3-5 show the plots for the first three passes of the simulated mission and display the most noteworthy features. The Earth and Sun azimuth angles (in the MAV staring frame) are shown as blue and orange dashed lines respectively. The evolution of the exclusion arcs for the Earth and Sun, centred on these lines, are shown by the corresponding blue and orange shaded regions. Note that in all cases due to the particular choice of $\mathbf{k}(t_0)$, at the start of each pass, the Earth azimuth is $\approx 90°$ with approximately the same exclusion arc width for each pass, corresponding to the same initial elevation of 20°. It can also be seen that at certain times the exclusion arcs shrink to zero

TABLE I: Simulated Mission Parameters

Parameter	Value
Altitude	500 km
Eccentricity e	0.001
Inclination	Sun-synchronous $\sim 97.5°$
LTAN	22:00
Mission duration	1 year (2026)
Ground station	53.3064° N, 6.2186° W (UCD)
Link min. elevation angle	20°

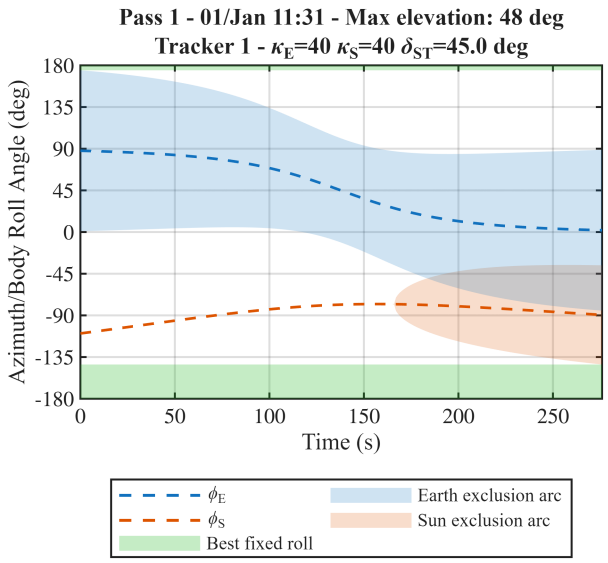

Fig. 3: Exclusion geometry and best fixed roll intervals for the first pass of the simulated mission.

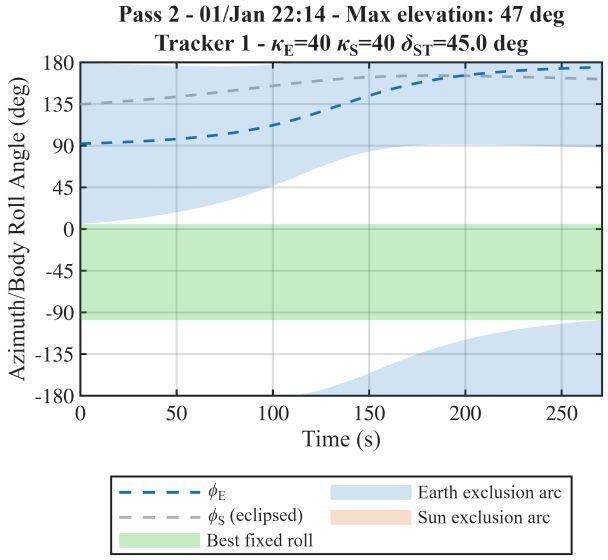

Fig. 4: Exclusion geometry and best fixed roll intervals for the second pass of the simulated mission.

width, when the exclusion zones for either Sun or Earth do not intersect the pointing circle. In Fig. 4 the dashed grey line for Sun azimuth shows that the Sun is eclipsed by the Earth for the full duration of the pass.

The Y-axis of these plots may be thought of as showing the star tracker pointing direction (body roll angle) over time. A roll trajectory which traverses such a plot from left to right, while avoiding the exclusion arcs (blue and orange shaded regions) guarantees star tracker availability. In this way, as alluded to earlier, the star tracker availability problem becomes a one-dimensional trajectory optimisation problem on the angle ϕ_B constrained by the combined exclusion arc boundaries. Fixed body roll angles (or intervals of roll angles)

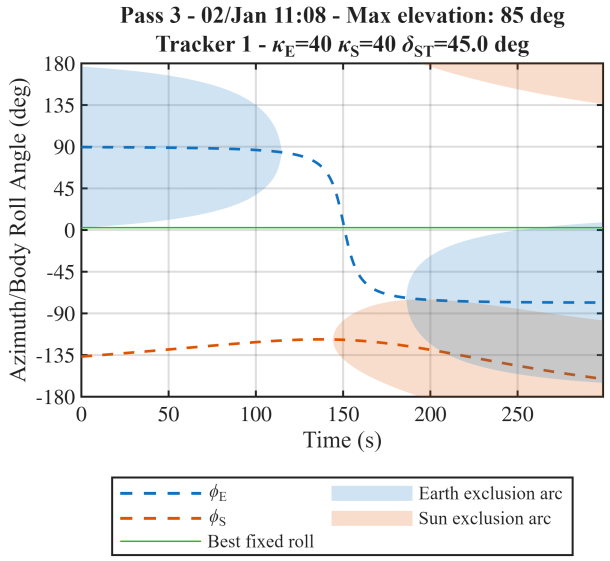

Fig. 5: Exclusion geometry and best fixed roll intervals for the third pass of the simulated mission.

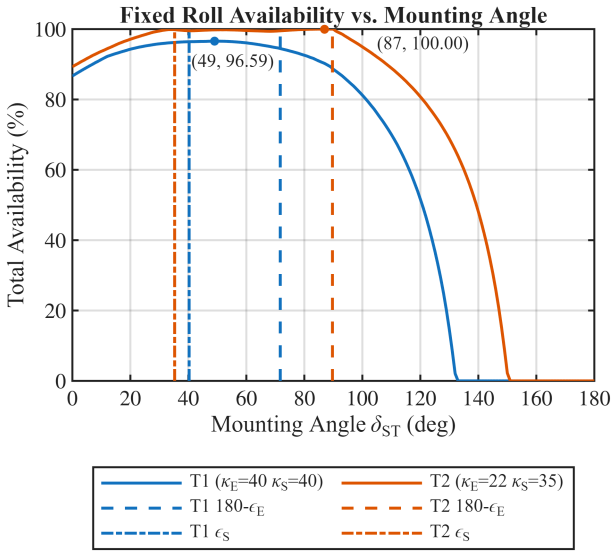

Fig. 6: Results showing total star tracker availability as a function of mounting angle for two candidate star trackers.

which maximise the availability over a pass are shown as green lines or green shaded regions. In the first two passes, it can be seen that the maximum availability is 100% and this availability is achieved over a range of roll angles (shaded region). In pass three 100% availability cannot be achieved and there is a single roll angle which maximises the availability over the pass (single line).

A second analysis was carried out to compare different candidate mounting angles $0 \geq \delta_{ST} \geq 180°$ for the star tracker. For this mounting angles over the full range in steps of $1°$ were tested. The analysis was carried out for two different star trackers with varying keep-out angle specifications: $(\kappa_S = 40°, \kappa_E = 40°)$ and $(\kappa_S = 35°, \kappa_E = 22°)$. Availability data was first calculated for each tracker, at each mounting angle, for each communication pass of the mission. Figure 6 shows a comparison of the total availability over the mission for the two candidate star trackers, versus the different mounting angles. The optimal mounting angle, which maximises availability is shown for each tracker. As expected the optimal mounting angle lies between the Sun keep-out angle and $180°$ minus the Earth keep-out angle, which are also shown. For small δ_{ST}, Sun exclusion dominates, while for large δ_{ST}, Earth exclusion becomes the limiting factor. The optimal mounting angle therefore lies between these extremes. The plot illustrates the effect of keep-out angle specifications for each tracker on availability. The trackers with larger keep-out angles experiences reduced availability and a narrower optimal mounting range, while the tracker with smaller exclusion constraints achieves close to 100% availability over a range of mounting angles. It should be noted that this study was limited to fixed roll trajectories. Considering time-varying roll trajectories over each communication pass may lead to greater availability.

VII. Conclusions

A framework has been presented for analysing and optimising spacecraft attitude trajectories during optical communication passes, with a particular emphasis on star tracker availability in the presence of Sun and Earth exclusion constraints. The case where the laser terminal is hard mounted on a CubeSat body is considered, where ground station tracking constrains two degrees of freedom of the spacecraft attitude. This paper focuses on the free third degree of freedom which corresponds to a roll about the laser boresight axis. By transforming the problem into a minimum angular velocity staring reference frame, the exclusion zones for Sun and Earth are reduced to exclusion arcs in the roll degree of freedom. This leads to a more intuitive one-dimensional trajectory optimisation problem over each communication pass.

As a first solution to this problem an algorithm is presented to determine optimal fixed-roll solutions. These solutions minimise the angular velocity and also torque about the roll axis in the axisymmetric case. By exploiting the piecewise-constant structure of the availability function under discrete time sampling, the optimal solution can be obtained by evaluating a finite set of candidate roll angles.

The methodology has also been extended to the optimisation of star tracker mounting angle over a full mission. Results demonstrate that the optimal mounting angle is bounded by competing Sun and Earth exclusion constraints, and that appropriate selection can significantly improve overall availability. This also demonstrated the effect on availability of different Sun and Earth keep-out angle specifications among candidate star trackers.

Future work will extend this approach to time-varying roll trajectories, formulated as an optimisation problem. This will enable the synthesis of feasible roll profiles in cases where fixed-roll solutions are not sufficient, while incorporat-

ing actuator limits, reaction wheel momentum management, and dynamic pointing constraints. The integration of these elements will provide a complete attitude planning framework for this type of optical communication mission.

REFERENCES

[1] K. Cahoy, P. Grenfell, A. Crews, M. Long, P. Serra, A. Nguyen, R. Fitzgerald, C. Haughwout, R. Diez, A. Aguilar, J. Conklin, C. Payne, J. Kusters, C. Sackier, M. LaRocca, and L. Yenchesky, "The CubeSat Laser Infrared CrosslinK Mission (CLICK)," in *International Conference on Space Optics — ICSO 2018*, N. Karafolas, Z. Sodnik, and B. Cugny, Eds. Chania, Greece: SPIE, Jul. 2019, p. 33.

[2] C. M. Schieler, K. M. Riesing, B. C. Bilyeu, B. S. Robinson, J. P. Wang, W. T. Roberts, and S. Piazzolla, "TBIRD 200-Gbps CubeSat Downlink: System Architecture and Mission Plan," in *2022 IEEE International Conference on Space Optical Systems and Applications (ICSOS)*. Kyoto City, Japan: IEEE, Mar. 2022, pp. 181–185.

[3] B. Rödiger, R. Rüddenklau, L. Elsner, T. Petermann, and P. Bangert, "First in-orbit results of the QUBE mission hosting a laser communication terminal for experiments towards quantum key distribution from CubeSats," 2025.

[4] K. Baeck, J. Wi, and H. Yoon, "Analytic pointing error evaluation on nano-satellite laser communication system," *Optics Communications*, vol. 559, p. 130419, May 2024.

[5] Y. Kim, P. Kim, H.-G. Ryu, S.-Y. Park, and S. Hall, "Performance Analysis of a Pointing, Acquisition, and Tracking System for the VISION Laser Crosslink Mission."

[6] B. Goeree and B. Shucker, "Geometric attitude control of a small satellite for ground tracking maneuvers," in *Proceedings of the Small Satellite Conference*, 1999.

[7] X. Chen, W. Steyn, and Y. Hashida, "Ground-target tracking control of Earth-pointing satellites," in *AIAA Guidance, Navigation, and Control Conference and Exhibit*. Dever,CO,U.S.A.: American Institute of Aeronautics and Astronautics, Aug. 2000.

[8] S. Han, J. Ahn, and M.-J. Tahk, "Analytical Staring Attitude Control Command Generation Method for Earth Observation Satellites," *Journal of Guidance, Control, and Dynamics*, vol. 45, no. 7, pp. 1347–1356, Jul. 2022.

[9] H. B. Hablani, "Attitude Commands Avoiding Bright Objects and Maintaining Communication with Ground Station," *Journal of Guidance, Control, and Dynamics*, vol. 22, no. 6, pp. 759–767, Nov. 1999.

[10] M. Tam and E. Glenn Lightsey, "Constrained spacecraft reorientation using mixed integer convex programming," *Acta Astronautica*, vol. 127, pp. 31–40, Oct. 2016.

[11] D. Beňo, P. Valábek, M. Hromčík, and M. Klaučo, "Star-Tracker-Constrained Attitude MPC for CubeSats," Apr. 2026.